

WOLF-RAYET GALAXIES IN THE SLOAN DIGITAL SKY SURVEY: THE METALLICITY DEPENDENCE OF THE INITIAL MASS FUNCTION

WEI ZHANG¹, XU KONG¹, CHENG LI¹, HONG-YAN ZHOU¹, FU-ZHEN CHENG¹

Draft version June 21, 2018

ABSTRACT

We use a large sample of 174 Wolf-Rayet (WR) galaxies drawn from the Sloan Digital Sky Survey to study whether and how the slope of the stellar initial mass function depends on metallicity. We calculate for each object its oxygen abundance according to which we divide our sample into four metallicity subsamples. For each subsample, we then measure three quantities: the equivalent width of H β emission line, the equivalent width of WR bump around 4650Å, and the WR bump-to-H β intensity ratio, and compare to the predictions of the same quantities by evolutionary synthesis models of Schaerer & Vacca. Such comparisons lead to a clear dependence of the slope of initial mass function (α) on metallicity in that galaxies at higher metallicities tend to have steeper initial mass functions, with the slope index ranging from $\alpha \sim 1.00$ for the lowest metallicity of $Z = 0.001$ to $\alpha \sim 3.30$ for the highest metallicity $Z = 0.02$. We have carefully examined the possible sources of systematic error either in models or in our observational measurements and shown that these sources do not change this result.

Subject headings: galaxies: abundances – galaxies: starburst – stars: Wolf-Rayet

1. INTRODUCTION

The stellar initial mass function (IMF) describes the relative frequency with which stars of various masses are formed, and so controls nearly all aspects of the evolution of stellar systems. An understanding of the IMF has thus long been one of the major goals in many astronomical fields, from theories of star formation to the interpretation of integrated properties of galaxies at the highest redshift.

The studies of IMF began with the publication of the first and still most famous paper on the subject by Salpeter (1955), who found that the solar neighborhood IMF can be approximated by a declining power law, $dN/dM \propto M^{-\alpha}$, with a slope of $\alpha = 2.35$. From then on, there have been considerable observational studies aiming to determine the form of the IMF (e.g. Scalo 1986, 1998; Kroupa 2001, 2002; Reid et al. 2002; Chabrier 2003). These studies have established that, for masses above $1 M_{\odot}$, the IMF can generally be quantified using the Salpeter form, while for low masses it deviates from this form, by flattening below $0.5 M_{\odot}$, peaking at a characteristic mass of $\sim 0.1 M_{\odot}$ and then significantly declining. However, despite much progress, there are still many problems that are far from being solved (Kennicutt 1998; Bate & Bonnell 2005), out of which the universality or the variation of the IMF is among the most fundamental and is still a controversial matter. In particular, it is not very clear whether or not the IMF, including both its characteristic mass around $0.1 M_{\odot}$ and its power-law slope at higher masses, depends on environmental conditions such as metallicity.

One reliable way to derive an IMF is to count individual stars when both photometry and spectroscopy are available. Massey et al. have applied this method to numerous young star clusters and OB associations in the Galaxy and the Magellanic Clouds (Massey et al. 1995, Massey 1999). This approach is, however, infeasible for deriving the starburst IMF because the distance of the closest starburst galaxies are $\gtrsim 2$ Mpc, where the spectrum of individual stars cannot be obtained. Thus the stellar content of galaxies at large distances

can only be derived from their integrated spectra (Leitherer 1998). In such studies, many authors have preferred to Wolf-Rayet (WR) galaxies, where broad emission lines from WR stars are observed in the integrated spectra. WR galaxies have long been known, beginning with the discovery of such features in the spectrum of the galaxy He 2-10 by Allen, Wright, & Goss (1976). Osterbrock & Cohen (1982), and Conti (1991) introduced the concept of WR galaxies. These galaxies are thought to be undergoing present or very recent star formation that produces massive stars evolving to the WR stage, and so are ideal objects for studying the early phases of starbursts, determining burst properties and constraining parameters of the IMF (Schaerer et al. 1999; Guseva et al. 2000).

Many studies have been done trying to constrain the main burst parameters, such as the age and duration of the bursts and the IMF, by comparing the observed WR features with that predicted by population synthesis models for young starbursts (Contini et al. 1999; Schaerer & Vacca 1998, hereafter SV98). These studies have produced some observational evidence in support of the variation of the IMF slope with metallicity. Schaerer et al. (1999) reported the detection of WC stars in five WR galaxies, of which three have metallicities of $Z = 0.004$ and the rest two have $Z = 0.008$ and $Z \gtrsim 0.020$ respectively. By comparing the observations with the model predictions of SV98, these authors found that only the two objects with higher metallicities are consistent with the standard model in which a Salpeter IMF is assumed, whereas the observed WR emission lines of the other three low metallicity objects can not be reproduced by this model and a flatter IMF is required in order to properly bring the models into agreement with the data. A study of three WR galaxies with $Z = 0.004$ by Huang et al. (1999) reached a similar conclusion that a top-heavy IMF with $\alpha = 1.00$ is likely required to favor the formation of WR stars in these low-metallicity galaxies. Recently, Schaerer et al. (2000) investigated six metal-rich WR galaxies ($Z \gtrsim 0.020$) and found that a very steep IMF with $\alpha \gtrsim 3.30$ is very unlikely for these objects. A more recent analysis of a larger sample of 14 WR galaxies by Fernandes et al. (2004) has concluded that there does exist some dependence of the IMF slope on galaxy metallicity. In

¹ Center for Astrophysics, University of Science and Technology of China, 230026, P. R. China

this study, low-metallicity galaxies are predicted to undergo a burst of star formation and show a flat IMF varying between the top-heavy and the Salpeter form, whereas high metallicity galaxies either show a steeper IMF or experience an extended burst.

The studies described above suggest that, at least for WR galaxies, the slope of the IMF is somewhat dependent on metallicity. However, the galaxy samples used in these previous studies are not sufficiently large to give reliable constraints on the relation between the IMF and the metallicity of galaxies. In this paper, we address this problem using a large sample of WR galaxies drawn from the Data Release Three (DR3; Abazajian et al. 2005) of the Sloan Digital Sky Survey (SDSS; York et al. 2000). SDSS is to date the most ambitious imaging and spectroscopic survey, providing a library of hundreds of thousands of galaxy spectra with a resolution of $\lesssim 3\text{\AA}$ at 5000\AA and a median signal-to-noise ratio (S/N) of ~ 14 per pixel. It thus has allowed one to select an unprecedented large, high quality spectral sample of WR galaxies, and subsequently to give reliable constraints on the relation between galaxy metallicity and the IMF slope.

From DR3, we select a large sample of 174 galaxies with obvious WR features using a two-step method, in which we first select star-forming galaxies with evident H ϵ emission and then select WR galaxies from these candidates by visually examining their spectra (§2). Next, for each WR galaxy we carefully calculate its oxygen abundance and measure its WR and H β emission, as quantified by the equivalent width (EW) of the WR bump around 4650\AA , the EW of H β emission line, and the WRbump/H β intensity ratio (§3). We then investigate the metallicity dependence of the IMF slope by comparing these observed quantities with those predicted by evolutionary synthesis models (§4). We discuss in §5 the possible biases in our results caused by a few sources of systematic error. Finally, we summarize our results in the last section.

2. SAMPLE SELECTION

2.1. The SDSS spectroscopic sample

The data analyzed in this study are drawn from the SDSS. The survey goals are to obtain photometry of one-quarter of the sky and spectra of nearly one million objects. Imaging is obtained in the u , g , r , i , z bands (Fukugita et al. 1996; Smith et al. 2002) with a special purpose drift scan camera (Gunn et al. 1998) mounted on the SDSS 2.5-meter telescope at Apache Point Observatory. The imaging data are photometrically (Hogg et al. 2001) and astrometrically (Pier et al. 2003) calibrated, and used to select stars, galaxies, and quasars for follow-up fibre spectroscopy. Spectroscopic fibres are assigned to objects on the sky using an efficient tiling algorithm designed to optimize completeness (Blanton et al. 2003). The details of the survey strategy can be found in York et al. (2000), and an overview of the data pipelines and products is provided in the Early Data Release paper (Stoughton et al. 2002). More details on the photometric pipeline can be found in Lupton et al. (2001).

Our parent sample for this study is composed of 374,767 objects which have been spectroscopically confirmed as galaxies and have data publicly available in the SDSS DR3. It is a catalogue of local galaxies (mostly below $z \approx 0.3$ and a median z of 0.1), covering 4188 deg^2 on the sky. The spectra are obtained with two 320-fibre spectrographs that are also mounted on the SDSS 2.5-meter telescope. Fibers with 3 arcsec in diameter are manually plugged into custom-drilled alu-

minum plates mounted at the focal plane of the telescope. The spectra are exposed for 45 minutes or until a fiducial S/N is reached. The median S/N per pixel for galaxies in the main sample is ~ 14 . The spectra cover an optical wavelength range from 3800 to 9200\AA with an instrumental resolution of $R = 1850 - 2200$ (FWHM $\sim 2.4\text{\AA}$ at 5000\AA).

2.2. Description of the selection method

We aim to select a sample of galaxies showing evident WR features in their spectra (blue bump around 4650\AA and/or red bump around 5808\AA). An intuitively accessible way is to systematically measure the EW of WR bumps and take those with large EWs as WR galaxies. However, this method will be extremely inefficient when dealing with large data sets, given that the WR galaxy population is just a very small fraction of the whole sample and in most cases systematical measurements of WR bump strength suffer from large uncertainties in the continuum determinations and/or from the contamination by the emission of non-WR stars.

To avoid this difficulty, we instead opt for a two-step method in which we first select star-forming galaxies with evident H ϵ emission line as candidates, and then select WR galaxies by visually examining these candidates. There is no denying that this method will inevitably drop a number of WR galaxies, especially those with low S/N. However, this method can still work well for our purpose, because of the following two facts. First, as described in the introduction, WR galaxies are believed to be undergoing present or very recent star formation that produces massive stars. It is then natural to speculate that a sample of WR galaxies must be a subsample of star-forming galaxies and most WR galaxies must show high-order Balmer emission lines in their spectra because these lines are usually associated with massive stars that are expected to be numerous in WR galaxies. We use the H ϵ emission line rather than other Balmer lines such as H δ in order to ensure that the high-excitation H II regions are selected. It should be pointed out that the H ϵ emission line is in fact a blend of three lines, including H ϵ , [Ne III] and He I lines. The latter two lines are often strong in active galactic nuclei (AGN). By using this blend we can find AGN with WR features in a harmonious way as normal galaxies, which are also interesting and will be discussed in a separated paper, at the cost of somewhat reducing our selection efficiency for the purpose of this paper. The second fact is that the parent sample is substantially large, allowing one to select a large enough sample of WR galaxies and thus to study their statistical properties still with unprecedented accuracy, even though some objects must have been thrown away.

2.3. Starlight removal and emission line measurements

To select star-forming galaxies, we have performed a careful subtraction of the stellar absorption-line spectrum before measuring the nebular emission lines. Our methodology for modelling and subtracting the underlying starlight has been described in detail in Li et al. (2005) and in Lu et al. (2006). The method for measuring the emission-line parameters has been described in Dong et al. (2005). A set of six absorption-line templates with zero velocity dispersion are constructed in the first place, by applying the technique of Independent Component Analysis to the synthesis galaxy spectra from a newly released high-resolution evolutionary model by Bruzual & Charlot (2003). The physical meaning of the six templates could be easily understood through examining their spectra

visually (see Fig.4 of Lu et al. 2006). The first template represents the blue continuum of O stars as well as the Ca II H and Ca II K lines at 3933Å and 3968 Å. The second template is similar to the spectrum of B stars, while the absorption lines of neutral metals and molecules such as TiO are also identified. The third template shows extremely strong Balmer absorption lines, a Balmer jump at the blue end, and the Ca II triplet and more lines of neutral metals and molecules at the red end. The fourth and fifth templates are somewhat like hybrids of F-K stars with stronger neutral metal and molecule lines. The last template is similar to the spectrum of M stars in the long-wavelength range but shows high-order Balmer absorption lines at short wavelengths. The spectral properties of the templates imply a tight correlation between the stellar population age and the templates (see Lu et al. 2006 for a detailed discussion). The spectra of all galaxies in the parent sample described above are then fitted with the six templates with iterative rejection of emission lines and bad pixels. During the modeling, the template spectra are broadened to velocity dispersion from 0 to 600 km s⁻¹ using Gaussian kernel, and an average intrinsic reddening is added to the model by searching a range of color excess $E(B-V)$ and assuming an extinction curve of Calzetti et al. (2000). For each spectrum, the best-fitting model is subtracted from the original spectrum, yielding a pure emission-line spectrum from which the emission-line parameters (the central wavelength, line intensity and line width) are measured.

As discussed in Li et al. (2005), our method of modeling and subtracting the underlying stellar component have several important advantages, and so the nebular emission lines can be accurately measured from the starlight-subtracted spectra. First, the templates are derived from a large sample with full coverage of spectral type. This ensures a very close match to the true underlying stellar population of different types of galaxies, including emission-line galaxies that contain much young stellar components. Second, the templates are not obtained directly from the observed spectra, but from the modeled one with zero velocity dispersion, and thus could well match the absorption-line profiles. Finally, all the emission lines with flux above 3σ are carefully masked during the modeling. This is vital to the nebular line measurements, especially for star forming galaxies. For each galaxy, the modeled spectrum is subtracted from the observed one, and the emission lines are fitted with Gaussian functions (see Dong et al. 2005 for details). Because emission lines and absorption lines are coupled, this procedure is performed iteratively.

2.4. Selecting WR galaxies

Based on the emission-line measurements, star-forming galaxies are selected from the subset of galaxies with the integrated flux intensity $F > 2 \times 10^{-17} \text{ erg s}^{-1} \text{ cm}^{-2}$ in the four emission lines [O III]λ5007, Hβ, [N II]λ6583 and Hα. Following Kauffmann et al. (2003), a galaxy is defined to be a star-forming galaxy if

$\log([\text{O III}]/\text{H}\beta) < 0.61/(\log([\text{N II}]/\text{H}\alpha) - 0.05) + 1.3$. (1)
This gives rise to a total of 117,275 star-forming galaxies.

The candidates of WR galaxies are then selected from these star-forming galaxies by requiring $\text{EW}(\text{H}\epsilon) > 5\sigma$, where $\text{EW}(\text{H}\epsilon)$ is the EW of Hε emission line and σ is its error. As a result, a total of 7628 galaxies are selected as our candidates. As described above, the spectra have been well fitted and the best-fitting stellar component (continuum plus absorption lines) has been separated from the emission-line component. Based on these fits, $\text{EW}(\text{H}\epsilon)$ and σ can be measured

in an easy and accurate manner. When measuring, we have adopted a rest-frame wavelength range of 3959Å to 3979Å for Hε. For each object, we use the best-fitting stellar spectrum (see §2.2), but not the observed spectrum, to determine the continuum that will be used for calculating the EW, in order to avoid possible contamination by nearby nebular emission lines. We have adopted 3905-3915Å for the nearby blue band and 4010-4030Å for the red. In the computation, the flux fluctuations provided by the SDSS pipeline have been taken into account.

Finally, we visually examine the spectra of the 7628 candidates and keep those with obvious WR features. This gives rise to a sample of 174 WR galaxies. In some cases, the selected WR galaxies show both the blue and red bumps, while in other cases only the blue bump is visible. We tabulate our sample in Table 1 so that the reader would be able to recover our results or perform other analyses using this sample. For each WR galaxy, we list in the table the spectroscopic ID (Column 1), the intensity ratio of various emission lines relative to Hβ emission line (Columns 2-18), the EWs of Hβ emission line (Column 20), the WRbump/Hβ intensity ratio (Column 21), the EWs of blue WR bump (Column 22) and the oxygen abundance (Column 23). Before these quantities being measured, the observed spectra have been corrected for the Galactic and the internal reddening (see the next section). The observed flux of Hβ emission line is listed in Column 19.

3. OBSERVATIONAL MEASUREMENTS

3.1. Correction of internal extinction

In the previous section, we have described our method for subtracting the underlying starlight and for measuring the emission lines. Before modelling the stellar spectrum of galaxies, the observed spectra have already been corrected for the Galactic reddening, but not for the internal reddening. The internal reddening can be estimated using the Balmer decrements of the emission lines from H II regions. We didn't apply this correction before the modelling, because our fitting method is aimed to model the stellar component of the galaxies, but not the H II regions where the gas dominates the observed spectrum. It has been known that the mean color excess estimated from the observed Balmer decrements is systematically larger than the average of the stellar extinction (Charlot & Fall 2000; Li et al. 2005). Therefore, we choose to take into account the stellar reddening by a single average color excess during the modelling. In this way our program attempts to fit the observed uncorrected spectra (continuum plus absorption lines). After the modelling, we measure emission-line parameters, correct for intrinsic extinction using Balmer decrements, and use the corrected parameters for further analysis. Our procedure of sample selection described above is not sensitive to this modification. However, when estimating metal abundance based on measurements of nebular emission lines, it is necessary to carefully correct for the internal reddening.

In practice, the internal reddening is usually corrected as a whole using the effective extinction curve $\tau_\lambda = \tau_V(\lambda/5500)^{-0.7}$, which was introduced by Charlot & Fall (2000). The effective V-band optical depth τ_V , arising from attenuation by dust in a galaxy, can be written

$$\tau_V = -\frac{\ln[F(\text{H}\alpha)/F(\text{H}\beta)] - \ln[I(\text{H}\alpha)/I(\text{H}\beta)]}{[(\lambda_{\text{H}\alpha}/5500)^{-0.7} - (\lambda_{\text{H}\beta}/5500)^{-0.7}]}, \quad (2)$$

where $F(\text{H}\alpha)/F(\text{H}\beta)$ is the ratio of the observed Hα emission intensity relative to Hβ, and $I(\text{H}\alpha)/I(\text{H}\beta)$ is the theoret-

TABLE 1
PARAMETERS OF THE WR SAMPLE.^d

MJD-Plate-Fib	Q	II	H10	H9	H8	H7	H δ	[O III] λ 4363	[O III] λ 4959	[O III] λ 5007	H α	[S II] λ 6717	[N I] λ 7774	[N I] λ 8446	[O II] λ 8446	H β	EW	WREW	12+	method			
372.7879883689979	108.3404363	4959	5007	656.3671	7673	1654865837	3207330486	1	(H β)ump	650g	(O/H)												
(1)	(2) ^a	(3)	(4)	(5)	(6)	(7)	(8)	(9)	(10)	(11)	(12)	(13)	(14)	(15)	(16)	(17)	(18)	(19) ^b	(20)	(21)	(22)	(23)	(24)
52251-0751-629...	...	6.1	19.629	927.850	4.7	6.4	164.0515	3280.89	1	6.2	1.4	4.1	4.2	1.9	847.366	7.5	1.3	8.01					Te
51900-0390-44391	42.6	5.3	17.828	724.817	7	3.6	151.2476	2285.47	913.6	7.2	20.7	2.3	1.91941	187.8	6.8	5.1	8.27					Te	
51900-0390-10806	9...	...	101.39	221.083	2	...	12.7	39.5286	67.930	335.7102	0.1	1	0.5	274.318	422.1	13.5	9.04					N2	
52233-0753-094	...	4.8	7.7	19.222	925.146	8	2.4	132.9418	2287.04	710.6	4.4	12.7	2.0	1.72323	51.7	17.3	7.9	8.33					Te
51817-0418-302	...	4.1	6.4	18.226	225.046	8	5.6	154.4485	8282.9	5.611	4.3	8.7	2.0	1.52271	679.4	7.1	5.1	8.05					Te
51913-0394-47293	3.9	6.1	16.728	724.945	3	11.1	172.9545	1278.48	2	6.1	1.3	3.7	1.1	1.0	723.886	8.2	2.7	2.1	7.80				Te
51789-0398-294	6.4	20.022	225.147	3	1.1	94.8	297.6289	624.116	9	6.7	19.2	2.2	2.31462	476.1	116.3	11.0	8.42				Te
51817-0399-32246	60.4	3.6	17.912	924.146	2	0.5	29.5	92.0288	137.829	730.085	8	1.8	1.6	975.633	8	7.0	2.0	8.09					Te
51882-0426-314	7.2	25.027	527.148	5	10.0	120.3379	5	...	9.3	7.2	0.9	2.6	1.4	0.7	989.893	11.4	2.4	7.51			Te
51900-0427-29225	20.1	2.4	16.912	422.343	3	1.6	64.4	201.6285	244.520	320.1	57.5	209.530	824.4	6.6	8.06					Te	

a) Columns 2-18 and 21 are intensity ratios relative to H β emission line, with $I(\text{H}\beta) = 100$. Before these quantities being measured, the observed spectra have been corrected for the Galactic reddening, the internal reddening and the stellar absorption. See the text for details.

b) The observed flux of H β emission line in unit of $10^{-17} \text{ erg s}^{-1} \text{ cm}^{-2}$, which has been corrected for the Galactic reddening, but not for the internal reddening.

c) Dots denote the cases in which H α or [O III] $\lambda\lambda$ 4959,5007 lines are clipped, or the corresponding lines are not detected.

d) Table 1 is presented in its entirety in the electronic edition of the Journal. A portion is shown here for guidance regarding its form and content.

ical value of this ratio. It has been known that $I(\text{H}\alpha)/I(\text{H}\beta)$ does not keep constant, but varies with electron temperature T_e , ranging from ~ 2.7 at $T_e = 20000\text{K}$ to ~ 3.0 at $T_e = 10000\text{K}$. In order to take this variation into account, we determine the electron temperature T_e using the observed intensity ratio $[\text{O III}]\lambda 4363/[\text{O III}]\lambda\lambda 4959, 5007$, from which we then calculate $I(\text{H}\alpha)/I(\text{H}\beta)$ using the method introduced by Storey & Hummer (1995). As a result, theoretical H α -to-H β ratios are successfully obtained for 152 WR galaxies whose T_e can be determined. In general, the observed H α /H β ratio is larger than the theoretical value, because H β emission is more heavily absorbed than H α . However, out of the 152 WR galaxies, there are 12 objects showing relatively smaller H α /H β ratios than theoretical values. This could be due to clipped H α lines or observational flux fluctuations. For these galaxies, we instead follow Izotov et al. (1994) to use H γ /H β intensity ratios to derive the extinction coefficient $C(\text{H}\beta)$ and the theoretical values of H γ /H β . In this way, 8 objects are corrected for the internal reddening. For the remaining 4 objects whose observed H γ /H β ratios larger than the theoretical values, we do not perform the correction.

For the 22 galaxies without T_e determinations, the correction of the internal reddening is performed in the same way, except that the theoretical intensity ratios are set to typical values of $I(\text{H}\alpha/\text{H}\beta) = 2.86$ (18 objects) or $I(\text{H}\gamma/\text{H}\beta) = 0.468$ (4 objects).

Fig. 1 compares the corrected hydrogen emission line ratios with the theoretical values for the galaxies that have T_e determinations and have been performed the correction based on the H α /H β intensity ratios. The crosses and filled circles show the observed and corrected ratios respectively. The lines are for the theoretical values. As can be seen, the intensity ratios of hydrogen lines H α , H γ and H δ relative to H β are corrected substantially and change to be consistent with the theoretical values.

Before going to the next section, it is necessary to find out the objects in our sample with clipped H α or [O III] $\lambda\lambda$ 4959,5007 lines in their spectra, because the oxygen abundance of galaxies will be determined based on these lines. By comparing the observed and/or corrected emission line ratios with the corresponding theoretical values, we find that 2 objects have been clipped for H α line, 1 for [O III] $\lambda\lambda$ 4959,5007, and 2 for both H α and [O III] $\lambda\lambda$ 4959,5007 lines.

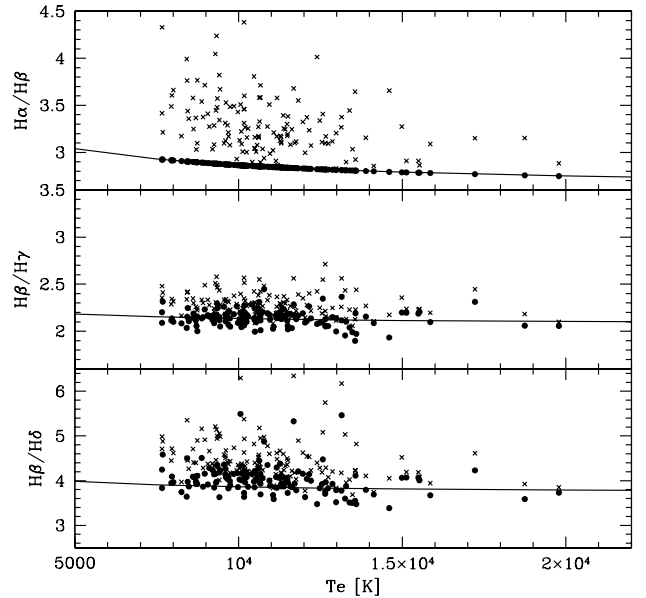


FIG. 1.— Intensity ratio of hydrogen emission lines as a function of electron temperature T_e , for WR galaxies in our sample that have been corrected for internal reddening. The observed ratios are plotted as crosses. The filled circles show the results that have been corrected for internal reddening using the method described in the text. The curves are for the theoretical values. [See the electronic edition of the Journal for the color version of this figure.]

3.2. Oxygen Abundance

There are several empirical methods that have been proposed to estimate the oxygen abundance of galaxies. In this paper we adopt two of them: the classic T_e method and the N2 method. In another paper (Shi et al. 2005), we have applied these methods to a sample of blue compact galaxies and discussed in detail the possible systematic differences among different methods. We present below a brief introduction to these methods and refer the reader to Shi et al. (2005) for a detailed description.

In the T_e method, one first determines the electron temperature T_e and density n_e of the gas using intensity ratios $[\text{O III}]\lambda 4363/[\text{O III}]\lambda\lambda 4959, 5007$ and

[S II] λ 6716/[S II] λ 6731 respectively, and then computes the abundances of O^+ and O^{+2} using the IRAF package NEBULAR (Shaw & Dufour 1995). In the computation, the O^+ abundance is determined by the intensity of [O II] λ 3727 line or [O III] λ 7320,7331, while the abundance of O^{+2} is determined by two [O III] lines centered at 4959 and 5007Å. Moreover, the fact that He II λ 4686 line is usually detected in the spectra of WR galaxies indicates that part of the oxygen in these systems must be in O^{+3} stage. Following Skillman & Kennicutt (1993), we estimate the O^{+3} abundance by assuming $O^{+3}/(O^+ + O^{+2}) \equiv He^{+2}/He^+$, where the helium abundances are determined using the He I λ 6678 and He II λ 4686 lines (Clegg 1987; Skillman & Kennicutt 1993). Therefore, the total abundance of oxygen in WR galaxies is derived by $O/H = (O^+ + O^{+2} + O^{+3})/H^+$ (Izotov et al. 1994; Skillman & Kennicutt 1993).

As mentioned above, we have determined the electronic temperature T_e for 152 out of 174 galaxies in our sample. We thus determine the oxygen abundance using the T_e method for these galaxies. In this procedure, the O^+ abundance is determined by the intensity of [O II] λ 3727 for 77 objects, while for the other 75 with the non-observed [O II] λ 3727 line, the [O III] λ 7320,7331 lines are used.

For the remaining 22 galaxies without T_e determinations, we have to turn to a second method, because some of the emission lines mentioned above, which are necessary in the T_e method, cannot be measured from their spectra due to the limited wavelength coverage (e.g. in case of [O II] λ 3727), the low S/N (e.g. in case of [O III] λ 4363) or clipping of [O III] λ 4959,5007. For these galaxies, we adopt the so-called $N2$ method (van Zee et al. 1998), in which the oxygen abundance is estimated by

$$12 + \log(O/H) = 1.02 \log[I([N II])/I(H\alpha)] + 9.36. \quad (3)$$

Where $I([N II])$ is $I([N II])(\lambda 6548 + \lambda 6583)$. It should be pointed out that for 3 objects whose $H\alpha$ lines are clipped, the $H\alpha$ fluxes are fixed to be $2.86 \times I(H\beta)$. We list in Table 1 the oxygen abundance for each object (Column 23) and the method adopted for it (Column 24).

As pointed out by Shi et al. (2005), the oxygen abundances derived from the $N2$ method are systematically larger by ~ 0.2 dex than those from the T_e method. We will show that this systematic difference does not affect our conclusion on the metallicity dependence of the IMF slope late.

3.3. The WR and $H\beta$ emission

In this paper we make comparisons with models for three quantities: the EW of $H\beta$ emission, the EW of WR bump around 4650Å (the blue bump), and the blue bump-to- $H\beta$ intensity ratio WRbump/ $H\beta$. As first pointed out by Copetti, Pastoriz, & Dottori (1986), the EWs of hydrogen recombination lines, particularly $H\beta$, can be used as an accurate indicator of the age of the population in the case of an instantaneous burst of star formation. In addition, as pointed out by SV98, EW($H\beta$) as a function of metallicity can be combined with WR lines/ $H\beta$ intensity ratios to determine the WR and O star populations. For the WR features, we concentrate on the blue bump only because this feature is visible in all the spectra (see §2.2).

We have described in detail our method of measuring $H\beta$ flux in §2.2 and the method of correcting for the effect of internal extinction in §3.1. The EW of $H\beta$ is measured in a similar way. However, The situation becomes difficult

when one trying to systematically measure the EW and intensity of WR bumps. As already mentioned in §2.2, systematical measurements of WR bump strength usually suffer from large uncertainties in the continuum determinations and/or from the contamination by the emission of non-WR stars such as [Fe III] λ 4658, He II λ 4686, He I+[Ar IV] λ 4711, and [Ar IV] λ 4740. We thus choose to manually measure the WR bump for all our WR galaxies. First, for each object, we use the best-fitting stellar spectrum, but not the observed spectrum, to determine the continuum. The continuum is then determined by fitting a cubic spline to seven wavelength channels (4020, 4510, 5313, 5500, 6080, 6630, 7043Å), which are thought to be fully free of nebular and stellar lines (Kong et al. 2002). Next, we fit the non-WR emission lines mentioned above with Gaussian functions and subtract them from the observed spectrum. We then measure the EW and the integrated flux of the blue bump with rest-frame wavelength limited to 4600-4750Å.

4. COMPARISON WITH MODEL PREDICTIONS

In this section, we compare the observed WR features and $H\beta$ emission with predictions by evolutionary synthesis models of SV98. In the comparison, we divide our sample into four subsamples according to oxygen abundance and investigate whether/how the slope of the IMF depends on galaxy metallicity. We first briefly describe the models, and then present the results of the comparison.

4.1. Predictions by Evolutionary Synthesis Models

The model predictions used in this paper are provided by SV98. These authors constructed evolutionary synthesis models for young starbursts, using stellar evolution models, theoretical stellar spectra, and a compilation of observed emission line strengths from WR stars. They explicitly distinguish between the various WR subtypes whose relative frequency is a strong function of metallicity. The observational features predicted by their models allow a detailed quantitative determination of the WR star population in a starburst region from its integrated spectrum and provide a means of deriving the burst properties (e.g. duration and age) and the slope of the IMF of young starbursts. The model predictions should provide the most reliable determinations to date, and can be used to investigate the variation in stellar properties with metallicity.

In the models, the input parameters include the burst duration Δt , the metallicity Z , the IMF, and the total mass of stars formed in the burst. As pointed out by SV98, the last parameter serves only as a normalization constant and is not relevant for the quantities being studied. For the IMF, a power law $dN/dM \propto M^{-\alpha}$ between the upper and low cutoff masses, M_{up} and M_{low} respectively, is adopted. Following SV98, we set the cutoff masses to $M_{up} = 120M_{\odot}$ and $M_{low} = 0.8M_{\odot}$. For the slope of the IMF, we consider three different cases: a Salpeter slope with $\alpha = 2.35$, a steeper slope with $\alpha = 3.30$, and a flatter slope with $\alpha = 1.00$. In each case, we assume an instantaneous burst with $\Delta t = 0$. In order to test the possible dependence on burst duration, we also consider in the case of Salpeter IMF four extended burst models with durations $\Delta t = 1, 2, 4$ and 10 Myr. Finally, in order to study the dependence on metallicity, we consider four cases of metallicity: $Z=0.001, 0.004, 0.008$, and 0.02.

With each set of input parameters, the models predict many important quantities which can be easily compared with observations. These quantities are classified into three groups:

population statistics (the number of stars with different spectral types), nebular quantities (the strength of nebular recombination lines: $H\alpha$, $H\beta$, $\text{He II}\lambda 4471$, and $\text{He II}\lambda 4686$), and WR emission lines. In this paper we study three of them: $\text{EW}(H\beta)$ (the EW of $H\beta$ emission line), $\text{EW}(4650)$ (the EW of the blue WR bump), and $\text{WRbump}/H\beta$ (the ratio of blue WR bump intensity relative to $H\beta$).

4.2. Metallicity dependence of the IMF

In order to study the metallicity dependence of the IMF and to make comparisons with the model predictions described above, we divide our sample into four subsamples according to oxygen abundance. Following Guseva et al. (2000), we assume the solar oxygen abundance $[12 + \log(\text{O}/\text{H})]_{\odot} = 8.93$ and use the oxygen abundance ranges listed below for the sample division.

1. $Z=0.001$: $12 + \log(\text{O}/\text{H}) \leq 7.93$;
2. $Z=0.004$: $7.93 < 12 + \log(\text{O}/\text{H}) \leq 8.43$;
3. $Z=0.008$: $8.43 < 12 + \log(\text{O}/\text{H}) \leq 8.63$;
4. $Z=0.020$: $12 + \log(\text{O}/\text{H}) > 8.63$.

Figure 2 shows the average spectrum of WR galaxies in each of the four metallicity subsamples. In the calculation, each observed spectrum is weighted by its S/N and normalized by the flux at 5000\AA . Panels from top to bottom correspond to different metallicities, as indicated in the left-hand panels. The number of objects included in each subsamples is also indicated. The panels at left-hand show the results obtained using the observed spectra that have been corrected only for Galactic reddening, while the right-hand panels are for those also corrected for the internal reddening. The inset in each panel shows the blue WR bump around 4650\AA . It can be seen that, if the internal extinction was not taken into account, low metallicity population shows harder continuum, as well as stronger nebular emission lines, than does high metallicity population. After the internal reddening being corrected for, the difference in the shape of the continuum disappears and the continuum slope changes to be very close to each other. This is reasonable because the dust content in high metallicity galaxies is expected to be larger than that in low metallicity ones. As a result, dust extinction will modify the continuum more significantly for high metallicities. It is also interesting to see that, the decrease of the strength of nebular emission lines does exist for large metallicities, regardless of whether the internal reddening is taken into account or not.

These observational results are shown more clearly in Figure 3, where we have plotted three quantities (from top to bottom: $\text{EW}(4650)$, $\text{EW}(H\beta)$ and $\text{WRbump}/H\beta$) as a function of oxygen abundance for all our WR galaxies (crosses). As expected, the observed $\text{WRbump}/H\beta$ intensity ratio decreases with decreasing metallicity. This result was first found by Arnault, Kunth, & Schild (1989) in an attempt to quantify the constraints on the WR populations in starbursts, and were largely confirmed by later studies. The result is believed to be due to the strong influence of metallicity on stellar mass loss, which leads to a significant decrease in the WR population at low metallicities (Maeder, Lequeux, & Azzopardi 1980). Moreover, the rapid decrease of $\text{EW}(H\beta)$ with increasing oxygen abundance is clearly seen from this figure. In contrast, we see no significant correlation between $\text{EW}(4650)$ and metallicity. The increase of $\text{WRbump}/H\beta$ with metallicity is thus

in large part due to the rapid decrease of $H\beta$ for large metallicities, which is well consistent with theoretical expectations (see below; also see Arnault et al. 1989).

Figure 3 also compares these quantities to predictions by the three instantaneous burst models with different IMFs ($\alpha = 1.00, 2.35, 3.30$) and metallicities ($Z = 0.001, 0.004, 0.008, 0.020$). We find that models with flatter IMFs tend to predict larger values for all these quantities and at all metallicities. This is reasonable because a flat IMF implies a relatively large population of massive stars, leading to strong WR and nebular emission. In particular, such metallicity dependence is much stronger in $\text{EW}(4650)$ and $\text{WRbump}/H\beta$ than in $\text{EW}(H\beta)$. We also see that the observed trends in the three quantities with oxygen abundance can generally be reproduced by all the models. However, the strength of the predicted trends is different for models with different IMFs. For example, a flatter IMF will lead to more rapid increase of $\text{WRbump}/H\beta$ with metallicity. As a result, the difference between model predictions becomes much more remarkable at high metallicities, reaching a factor of ~ 5 in $\text{EW}(4650)$ and ~ 3 in $\text{WRbump}/H\beta$ on average at $Z > Z_{\odot}$. It is thus inevitably to see that a model with a fixed IMF can not simultaneously match the observations at all metallicities. At the highest metallicity ($Z = 0.02$), only the model with the steepest IMF ($\alpha = 3.30$) can well match the observed $\text{EW}(4650)$ and $\text{WRbump}/H\beta$. In case of $Z = 0.001$, however, just the reverse is likely to be true. In another word, Fig. 3 indicates that a dependence of the IMF slope on galaxy metallicity is required to explain the observed trends in WR and $H\beta$ emission.

Figures 4 and 5 (black points in the top panels) show the distribution in spaces of $\text{EW}(4650)$ versus $\text{EW}(H\beta)$ and $\text{WRbump}/H\beta$ versus $\text{EW}(H\beta)$ respectively, for WR galaxies in different metallicity subsamples (as indicated above each panel). In each panel, the average location of the objects is plotted as a green point and the 1σ dispersion between them is indicated by the error bars. The solid lines show the predictions by the three instantaneous burst models, with red, magenta and blue colours respectively corresponding to models with IMF slope $\alpha = 1.00, 2.35$ and 3.30 . The magenta lines in other styles are for the four extended burst models with fixed IMF slope ($\alpha = 2.35$), but various burst durations: $\Delta t = 1$ (dotted), 2 (dashed), 4 (long dashed), 10 Myr (dotted-dashed). A clear dependence of the IMF slope on metallicity can be seen from the two figures, in that WR galaxies with higher metallicities exhibit steeper IMF. As can be seen, most objects with $Z = 0.02$ are located well below the $\alpha = 3.30$ curve, implying that these galaxies have IMFs similar to or even steeper than the steepest IMF that we have probed. In contrast, the objects of $Z = 0.001$ are dominantly above the $\alpha = 1.00$ curve, and so should be associated with very flat IMFs. At intermediate metallicities, the scatter in the observational distributions is very large, but the observations are still on average consistent with the Salpeter IMFs, the ones having the intermediate slope.

5. SOURCES OF SYSTEMATIC ERROR

In the previous section, we have seen a clear dependence of the IMF slope on metallicity by comparing our measurements of WR features and $H\beta$ with the model predictions provided by SV98. However, there are possible uncertainties in this result, caused by a few sources of systematic error either in the models or in the observational measurements. We discuss these in detail in this section.

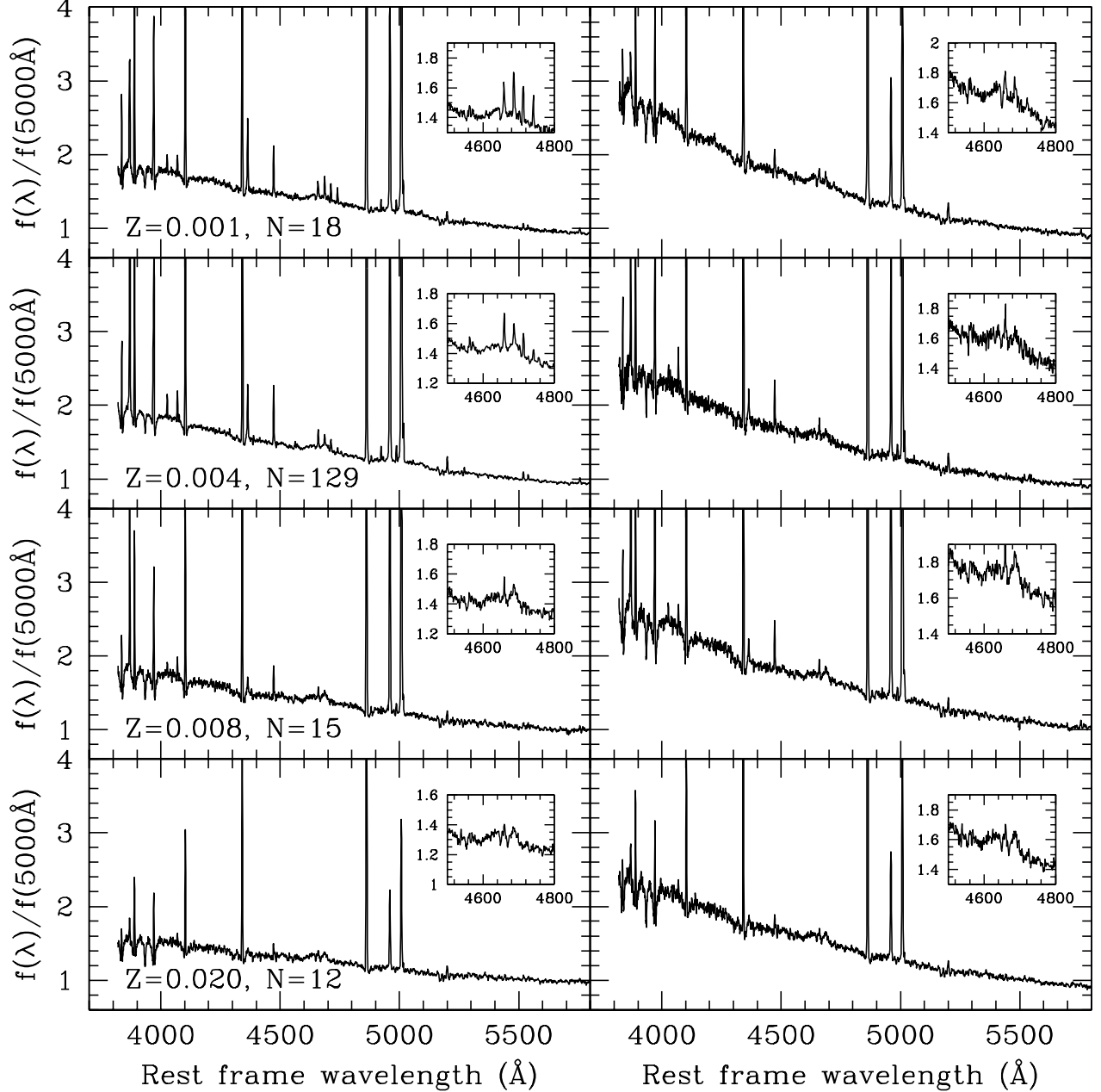


FIG. 2.— Average spectrum of WR galaxies in different metallicity subsamples. Panels from top to bottom correspond to different metallicities, as indicated in the left-hand panels. The number of objects in each subsample is also indicated. The panels at left-hand are for the results obtained from the observed spectra that have been corrected only for Galactic reddening, whereas the right-hand panels are for those also corrected for the internal reddening. The inset in each panels shows the WR bump around 4650Å.

5.1. Aperture effects

Each of the SDSS spectra was obtained using a 3 arcsecond diameter fibre that had been positioned as close as possible to the centre of the object being studied. One may thus wonder to what extent our measurements of $\text{EW}(4650)$, $\text{EW}(\text{H}\beta)$ and $\text{WRbump}/\text{H}\beta$ may be biased because the measurements are not accurately reflecting the stellar and gaseous content of the whole starburst region. For example, because of aperture effects, both $\text{EW}(4650)$ and $\text{EW}(\text{H}\beta)$ may be somewhat underestimated. As a result, the locations of galaxies on each

panel of Figure 4 may be biased toward lower-left corner and thus mismatch the theoretical curves.

In order to address the effect of aperture bias, we define a subsample of “safe” objects as those fully enclosed within the spectroscopic aperture. We use the Petrosian radii in the five SDSS photometric bands provided by the SDSS pipeline to quantify the angular size and select “safe” objects by requiring that at least one of the five radii is smaller than the radius of the aperture. This results in a subsample of 23 WR galaxies whose spectra are not suffering from the aperture effect.

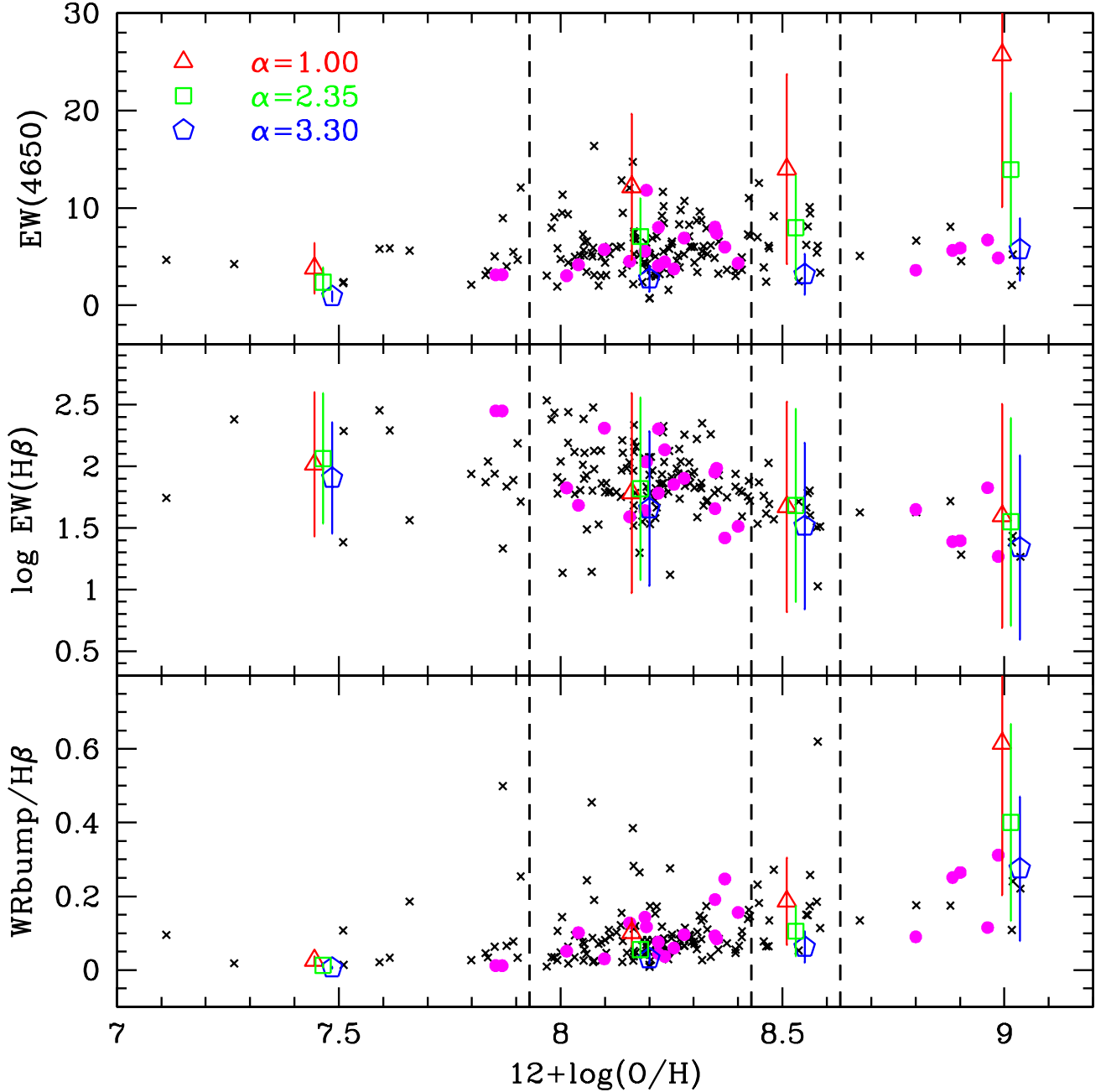


FIG. 3.— Equivalent width (EW) of WR bump around 4650\AA (top), EW of $H\beta$ emission line (median), and the intensity ratio of WR bump relative to $H\beta$ (bottom) are plotted as a function of oxygen abundance. The crosses are for all the WR galaxies in our sample, while the filled circles are for “safe” objects, defined as those with at least one of the five Petrosian radii smaller than the radius of the SDSS spectroscopic aperture ($1.5''$). The symbols with error bars show the average values with $1-\sigma$ variance, which are predicted by models with different IMF slopes, as indicated in the top panel. Dashed vertical lines denote the oxygen abundance ranges and the model predictions are plotted at the median of each range. For clarity, triangles, squares and pentagons are slightly shifted along the horizontal axis.

Though much smaller in size, this subsample will provide a critical test on the results obtained from the whole sample.

In Figure 3, the “safe” objects are highlighted as filled circles. In case of $EW(4650)$, it is likely that there is no significant bias in the whole sample relative to the “safe” sample. In contrast, a fraction of the whole sample shows much smaller $EW(H\beta)$ compared to the “safe” sample. We thus conclude that all emission of WR stars is likely inside the fi-

bre, whereas aperture bias could well be a problem for $H\beta$. This can be understood as $H\beta$ emission is more extended. As a result, $WRbump/H\beta$ intensity ratio is overestimated to varying degrees for some of the objects.

The relations between the three quantities obtained from the “safe” sample are plotted in the second rows of panels of Figures 4 and 5. The symbols and the lines are the same as in top panels and the number of objects included in each metallicity

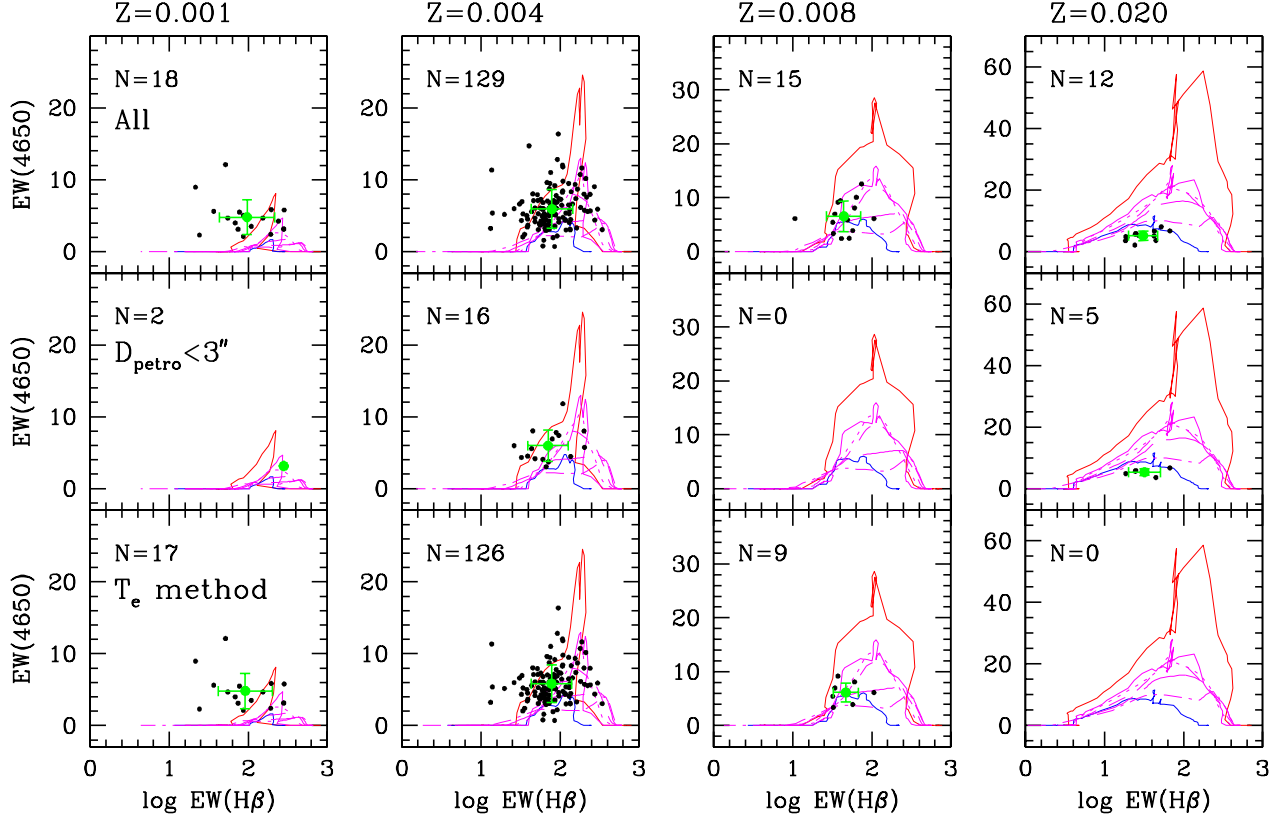


FIG. 4.— Distribution in the space of $EW(4650)$ versus $EW(H\beta)$ for WR galaxies in different metallicity subsamples (black points). Panels from left to right correspond to different metallicities, as indicated above the top panels. The top panels are for the whole sample. The median panels are for objects with at least one of the five Petrosian radii smaller than the radius of the SDSS spectroscopic aperture. The bottom panels are for objects with their oxygen abundances determined from T_e method. In each panel, the average location of the objects is plotted as a green point and the $1-\sigma$ dispersion between them is indicated by the error bars. The solid lines show the predictions by the three instantaneous burst models, with red, magenta and blue colours, respectively, corresponding to models with IMF slope $\alpha=1.00$, 2.35 and 3.30 . The magenta lines in other styles are for the four extended burst models with fixed IMF slope ($\alpha=2.35$) but various burst durations: $\Delta t=1$ (dotted), 2 (dashed), 4 (long dashed), 10 Myr (dotted-dashed).

subsample is also indicated. It is encouraging to see that the metallicity dependence of the IMF slope still exists. We are thus convinced that the effects of aperture do not change our main results.

5.2. Oxygen abundance

In our sample, the oxygen abundance of 152 objects is determined from the T_e method, while for the others we have adopted the $N2$ method. As mentioned above, the measurements based on the $N2$ method are systematically larger than those based on the T_e method, by a factor of ~ 0.2 dex. Moreover, for 27 galaxies with $[O\ III]\lambda 4959/H\beta < 0.7$, the EW of $H\beta$ is generally low and the $[O\ III]\lambda 4363$ line is weak, hence their oxygen abundances might be underestimated (Izotov et al. 2004). It is thus necessary to test how reliable the methods are and whether and how they affect our main results.

For T_e method, it is possible to address this problem in a statistical way by comparing the Ne/O , S/O and Ar/O abundance ratios and the average values found for galaxies with different oxygen abundances. If these ratios are not consistent with the average values, the metallicity might be somewhat underestimated (e.g. Izotov et al. 2004). Adopting a two-zone photoionized H II region model described by Izotov, Thuan, &

Lipovetsky (1994), for each of the 152 objects whose oxygen abundances are determined from the T_e method, we calculate its Ne^{++}/O^{++} , S^{+} and S^{++} using expressions from Pagel et al. (1992), and Ar^{++} , Ar^{+++} using IRAF NEBULAR package (see Shaw & Dufour 1995). We then calculate their Ne/O , S/O and Ar/O abundance ratios, using the ionization correction factors (ICFs) presented by Izotov, Thuan, & Lipovetsky (1994). The results are shown in Figure 6. The dotted lines are for the average values found by Izotov & Thuan (1999). It is seen that the abundance ratios are well consistent with the average values at all oxygen abundances.

Figure 6 demonstrates that our calculation of oxygen abundance based on the T_e method is reliable and robust. We thus select the 152 objects with oxygen abundance determined from the T_e method to construct a second "safe" sample, in order to exclude any possible biases in our results caused by the $N2$ method. Similarly, we plot the results for this "safe" sample in the third rows of panels of Figures 4 and 5 and obtain a conclusion that our results are not significantly biased by the uncertainties in oxygen abundance determinations. Note that there are no objects included in the $Z = 0.020$ subsample. This is due to the fact that the application of T_e method requires an accurate determination of the $[O\ III]\lambda 4363$ inten-

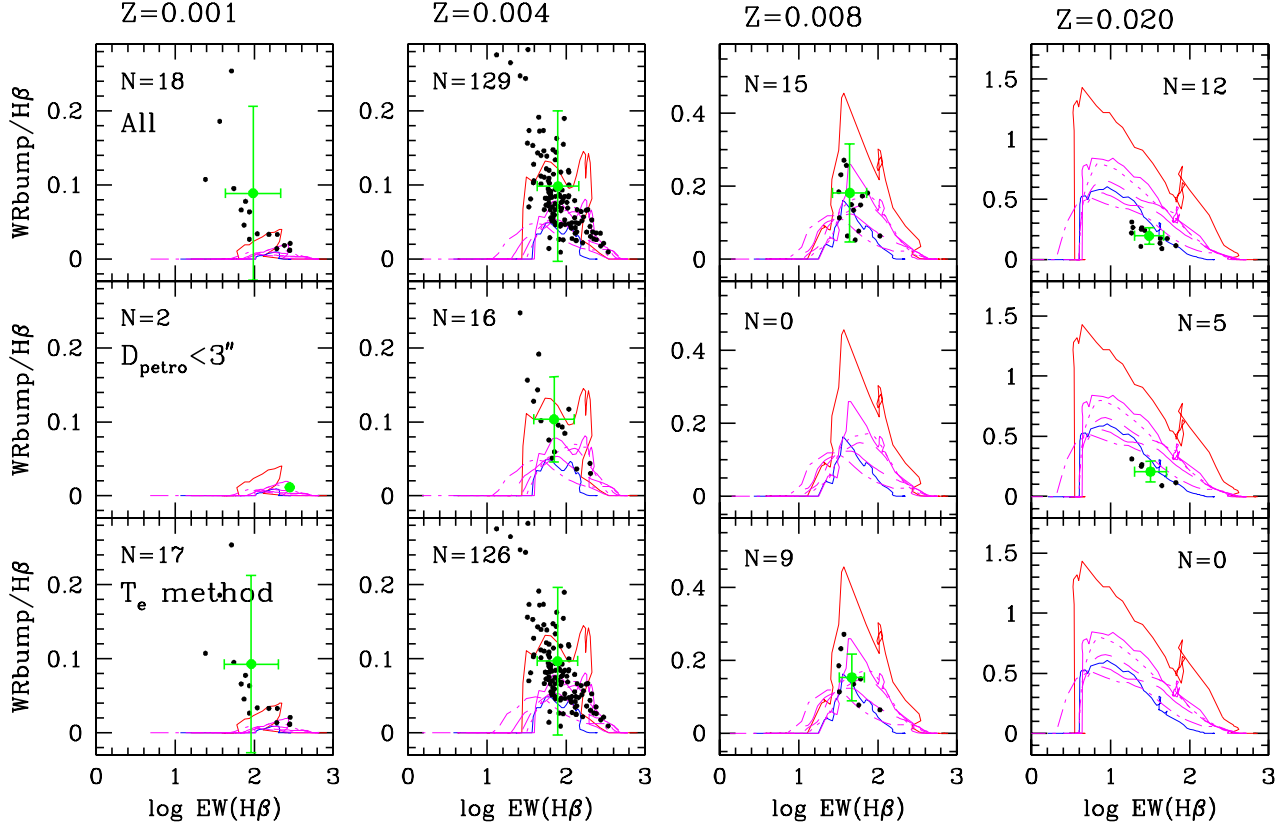


FIG. 5.— Distribution in the space of $WR_{bump}/H\beta$ versus $EW(H\beta)$, for WR galaxies in different metallicity subsamples. The symbols and the lines are the same as in Figure 4.

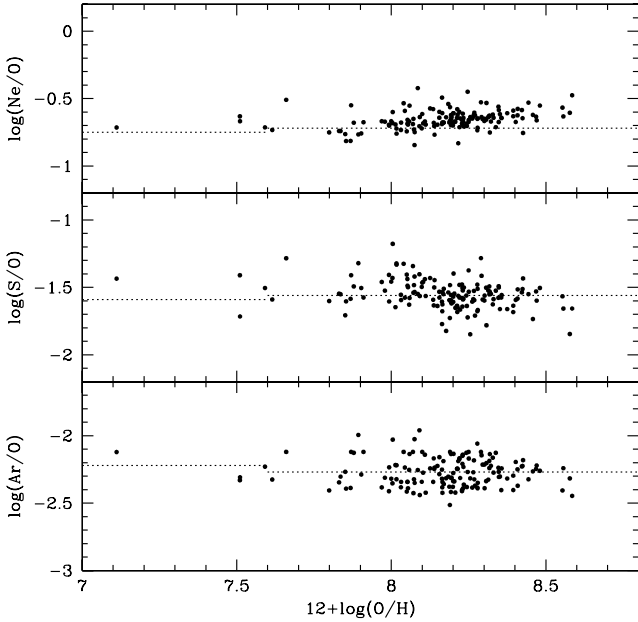


FIG. 6.— The Ne/O , S/O , and Ar/O abundance ratios of 152 WR galaxies whose oxygen abundance are determined from the T_e method.

sity, but in general this line is very weak or invisible in the spectra of high-metallicity galaxies. Nevertheless, the rest three panels still show marked increase of IMF slope with increasing metallicity, and thus our conclusion about the metallicity dependence keeps unchanged.

5.3. Spectral modelling

In this paper, the EWs are measured adopting the best-fitting stellar continuum. However, the contribution of the ionized gas emission could be high in H II regions, especially for those with high $EW(H\beta)$. The most recent paper by Gu-seva et al. (2006), where the ionized gas emission is considered in the fitting procedure, shows that the flux fraction of the gaseous continuum near $H\beta$ can reach $\sim 50\%$ in H II regions with $EW(H\beta) \sim 400\text{\AA}$. Therefore, the ionized gas continuum template should be included in the spectral modelling, otherwise the EWs will be underestimated. Since our templates are constructed from simple stellar populations, our method currently can not be able to include the gas continuum in the fitting. Moreover, the absolute majority of our sample are low redshift objects in which the Balmer continuum is not within the SDSS wavelength coverage. It is thus very difficult to break the degeneracy between gaseous continuum and very young stellar populations only using the optical spectra without this feature.

In addition, the measured EWs are compared with the model predictions for instantaneous or short bursts, and thus

the EWs should be obtained adopting the continuum level only of the youngest template that is most likely associated with the WR stars. Therefore, adopting the best-fitting stellar continuum will also lead to underestimated EWs. If the ratio of the youngest template continuum to the total one systematically varies at different metallicities, then the results shown in Figures 4 and 5 may also be biased. We have checked the relative contributions to the best-fitting spectra by the first two templates, which roughly represent the spectra of O and B stars respectively (see §2.3), and found no tendency of these contributions with metallicity. Therefore, although the EWs have somewhat been underestimated, the overall correlation between the measured EWs and the metallicities can still exist and thus the trend of the IMF slope with metallicity can still be true.

5.4. Synthesis models

In this paper, the theoretical predictions are made using the evolutionary synthesis models of SV98. It is worthy noticing that their models are based on the evolution of non-rotating stars. Stellar rotation is expected to predict longer WR stage, lower WR star masses, and thus larger WR populations. As mentioned above, the strong influence of metallicity on stellar mass loss leads to a significant decrease in the WR population at low metallicities, resulting in rapid decrease of WRbump/H β intensity ratio at these metallicities. Therefore, if rotating stars are included in the models, both EW(4650) and WRbump/H β would be larger than that predicted by the current models. As a result, the predicted curves in the low-metallicity panels of Figures 4 and 5 would go upward, and the observed decrease of the IMF slope at low metallicities would be less pronounced. New models of rotating stars are thus needed to be worked out, in order to provide more reliable predictions, especially for low-metallicity populations.

Moreover, SV98 have compiled average line fluxes for WR stars in the LMC (for models with $Z < Z_{\odot}$) or the Galaxy (for models with $Z > Z_{\odot}$), which represent the standard calibration for WR populations in external galaxies. There has, however, been a recent study of the luminosities of WR emission lines, reaching the indication that WR stars at SMC metallicities possess lower optical line luminosities than those in the LMC (Crowther & Hadfield 2006). This could be another source of systematic error which may also leads to underpredicted WR populations.

It is thus important to answer the questions that to what extent the two effects described above would change the predictions at low metallicities and which effect should be more dominant in such bias. However, at the moment, there are no published evolutionary synthesis models with rotating stars and more recent WR line luminosities. Nevertheless, one can still expect that these effects do not significantly change the results at high metallicities, for which the observed metallicity dependence of the IMF slope can still exist.

6. SUMMARY

In this paper, we have analyzed the WR features and H β emission of 174 WR galaxies drawn from the Sloan Digital Sky Survey. By comparing these observed quantities with predictions by evolutionary synthesis models of Schaerer & Vacca (1998), we investigate whether and how the stellar initial mass function depends on metallicity. Our sample is constructed using a two-step method, in which we first select candidates as the star-forming galaxies with evident He emission lines and then select WR galaxies by visually examine

the spectra of the candidates. Although this method has inevitably exclude a number of objects (mainly with low S/N), it is still work well for our purpose and gives rise to a large enough, high quality sample of WR galaxies. We have carefully examine the possible sources of systematic error either in models or in our observational measurements and shown that these sources do not change our main results.

The conclusions of this paper can be summarized as follows.

1. The continuum of the average spectrum of WR galaxies shows no significant dependence on metallicity. In contrast, low-metallicity galaxies exhibit in their spectra much stronger nebular emission than high-metallicity galaxies.
2. The observed equivalent width (EW) of H β decreases with increasing metallicity, whereas there is no significant trend in EW of WR blue bump around 4650Å with metallicity.
3. We have found a clear dependence of the IMF slope on metallicity in that the IMF slope increases with increasing metallicity. Such dependence has been probed by many previous studies, but it is much more pronounced in this paper due to the improvement in the observational data.

It should be pointed out that there is still room for improvement of this study. First, the method of sample selection could be developed as to fully take advantage of the large number of SDSS galaxies. Second, more accurate measurements of WR lines and new models incorporating stellar rotation are needed to refine the results, especially for low metallicities. Third, the aperture effects should be corrected in a statistically robust way incorporating the stellar contents obtained in our starlight fitting procedure and the method of spectral modelling could be improved. Finally, more quantities such as the relative numbers of WR stars with different subtypes could be included in the comparison to give more subtle and convincing results. These will be the aims of subsequent papers.

We thank the anonymous referee for useful and constructive comments that resulted in a significant improvement of this paper. We are grateful to Dr. Daniel Schaerer for providing the model predictions and for his helpful comments. We thank the SDSS teams for making their data publicly available, and Dr. Yuri I. Izotov for helpful discussion. This work is supported by the Chinese National Science Foundation through NSF10573014, NSF10633020, and by the Bairen Project of the Chinese Academy of Sciences.

Funding for the SDSS and SDSS-II has been provided by the Alfred P. Sloan Foundation, the Participating Institutions, the National Science Foundation, the U.S. Department of Energy, the National Aeronautics and Space Administration, the Japanese Monbukagakusho, the Max Planck Society, and the Higher Education Funding Council for England. The SDSS is managed by the Astrophysical Research Consortium for the Participating Institutions. The Participating Institutions are the American Museum of Natural History, Astrophysical Institute Potsdam, University of Basel, Cambridge University, Case Western Reserve University, University of Chicago, Drexel University, Fermilab, the Institute

for Advanced Study, the Japan Participation Group, Johns Hopkins University, the Joint Institute for Nuclear Astrophysics, the Kavli Institute for Particle Astrophysics and Cosmology, the Korean Scientist Group, the Chinese Academy of Sciences (LAMOST), Los Alamos National Laboratory,

the Max-Planck-Institute for Astronomy (MPIA), the Max-Planck-Institute for Astrophysics (MPA), New Mexico State University, Ohio State University, University of Pittsburgh, University of Portsmouth, Princeton University, the United States Naval Observatory, and the University of Washington.

REFERENCES

- Abazajian, K., et al. 2005, *AJ*, 129, 175
 Allen, D. A., Wright, A. E., & Goss, W. M. 1976, *MNRAS*, 177, 91
 Arnault, P., Kunth, D., & Schild, H. 1989, *A&A*, 224, 73
 Bate, M. R., & Bonnell, I. A. 2005, *MNRAS*, 356, 1201
 Blanton, M. R., Lin, H., Lupton, R. H. et al. 2003, *AJ*, 125, 2276
 Bruzual, G., & Charlot, S. 2003, *MNRAS*, 344, 1000
 Calzetti, D., Armus, L., Bohlin, R. C. et al. 2000, *ApJ*, 533, 682
 Chabrier, G. 2003, *PASP*, 115, 763
 Charlot, S., & Fall, S. M. 2000, *ApJ*, 539, 718
 Clegg, R. E. S. 1987, *MNRAS*, 229, 31P
 Conti, P. S. 1991, *ApJ*, 377, 115
 Contini, T., Schaerer, D., & Kunth, D. 1999, *IAU Symp.* 193: Wolf-Rayet Phenomena in Massive Stars and Starburst Galaxies, 193, 578
 Copetti, M. V. F., Pastoriza, M. G., & Dottori, H. A. 1986, *A&A*, 156, 11
 Crowther, P. A., & Hadfield, L. J. 2006, *A&A*, 449, 711
 Dong, X.-B., Zhou, H.-Y., Wang, T.-G. et al. 2005, *ApJ*, 620, 629
 Eisenhauer, F. 2001, *Science with the Large Binocular Telescope*, 89
 Fernandes, I. F., de Carvalho, R., Contini, T., & Gal, R. R. 2004, *MNRAS*, 355, 728
 Fukugita, M., Ichikawa, T., Gunn, J. E. et al. 1996, *AJ*, 111, 1748
 Gunn, J. E., et al. 1998, *AJ*, 116, 3040
 Guseva, N. G., Izotov, Y. I., & Thuan, T. X. 2000, *ApJ*, 531, 776
 Guseva, N. G., Izotov, Y. I., & Thuan, T. X. 2006, *ApJ*, 644, 890
 Hogg, D. W., Finkbeiner, D. P., Schlegel, D. J., & Gunn, J. E. 2001, *AJ*, 122, 2129
 Huang, J. H., Gu, Q. S., Ji, L. et al. 1999, *ApJ*, 513, 21
 Izotov, Y. I., Stasińska, G., Guseva, N. G., & Thuan, T. X. 2004, *A&A*, 415, 87
 Izotov, Y. I., & Thuan, T. X. 1999, *ApJ*, 511, 639
 Izotov, Y. I., Thuan, T. X., & Lipovetsky, V. A. 1994, *ApJ*, 435, 64
 Kauffmann, G., et al. 2003, *MNRAS*, 346, 1055
 Kennicutt, R. C., Jr. 1998, *ASP Conf. Ser.* 142: The Stellar Initial Mass Function (38th Herstmonceux Conference), 142, 1
 Kong, X., Cheng, F. Z., Weiss, A., & Charlot, S. 2002, *A&A*, 396, 503
 Kroupa, P. 2001, *MNRAS*, 322, 231
 Kroupa, P. 2002, *Science*, 295, 82
 Leitherer, C. 1998, *ASP Conf. Ser.* 142: The Stellar Initial Mass Function (38th Herstmonceux Conference), 142, 61
 Li, C., Wang, T.-G., Zhou, H.-Y. et al. 2005, *AJ*, 129, 669
 Lu, H., Zhou, H., Wang, J. et al. 2006, *AJ*, 131, 790
 Lupton, R., Gunn, J. E., Ivezić, Z. et al. 2001, *ASP Conf. Ser.* 238: Astronomical Data Analysis Software and Systems X, 238, 269
 Maeder, A., Lequeux, J., & Azzopardi, M. 1980, *A&A*, 90, L1
 Massey, P. 1999, *IAUSymp.* 190: New Views of the Magellanic Clouds, 190, 173
 Massey, P., Lang, C. C., Degioia-Eastwood, K., & Garmany, C. D. 1995, *ApJ*, 438, 18
 Osterbrock, D. E., & Cohen, R. D. 1982, *ApJ*, 261, 64
 Pier, J. R., Munn, J. A., Hindsley, R. B. et al. 2003, *AJ*, 125, 155
 Reid, I. N., Gizis, J. E., & Hawley, S. L. 2002, *AJ*, 124, 2721
 Salpeter, E. E. 1955, *ApJ*, 121, 161
 Scalo, J. M. 1986, *Fundamentals of Cosmic Physics*, 11, 1
 Scalo, J. 1998, *ASP Conf. Ser.* 142: The Stellar Initial Mass Function (38th Herstmonceux Conference), 142, 201
 Schaerer, D., Guseva, N. G., Izotov, Y. I., & Thuan, T. X. 2000, *A&A*, 362, 53
 Schaerer, D., Contini, T., & Kunth, D. 1999, *A&A*, 341, 399
 Schaerer, D., & Vacca, W. D. 1998, *ApJ*, 497, 618 (SV98)
 Shaw, R. A., & Dufour, R. J. 1995, *PASP*, 107, 896
 Shi, F., Kong, X., Li, C., & Cheng, F. Z. 2005, *A&A*, 437, 84
 Skillman, E. D., & Kennicutt, R. C., Jr. 1993, *ApJ*, 411, 655
 Smith, J. A., et al. 2002, *AJ*, 123, 2121
 Storey, P. J., & Hummer, D. G. 1995, *MNRAS*, 272, 41
 Stoughton, C., et al. 2002, *AJ*, 123, 485
 van Zee, L., Salzer, J. J., Haynes, M. P. et al. 1998, *AJ*, 116, 2805
 York, D. G., et al. 2000, *AJ*, 120, 1579